



RESEARCH LETTER

10.1029/2023GL104313

Climate Base State Influences on South Asian Monsoon Processes Derived From Analyses of E3SMv2 and CESM2

Key Points:

- Base state differences in Energy Exascale Earth System Model version 2 (E3SMv2) compared to Community Earth System Model version 2 (CESM2) include cooler tropical Indian and Pacific sea surface temperatures (SSTs) and reduced ENSO amplitude
- Base state differences in the two models do not appreciably affect simulations of the regional patterns of South Asian monsoon precipitation
- Cooler SSTs and lower amplitude ENSO in E3SMv2 combine to contribute about equally to weaker monsoon-ENSO teleconnections compared to CESM2

Supporting Information:

Supporting Information may be found in the online version of this article.

Correspondence to:

G. A. Meehl,
meehl@ucar.edu

Citation:

Meehl, G. A., Shields, C. A., Arblaster, J. M., Neale, R., Hu, A., Annamalai, H., et al. (2023). Climate base state influences on South Asian monsoon processes derived from analyses of E3SMv2 and CESM2. *Geophysical Research Letters*, 50, e2023GL104313. <https://doi.org/10.1029/2023GL104313>











Received 28 APR 2023
Accepted 21 AUG 2023

Author Contributions:

Conceptualization: Gerald A. Meehl
Data curation: Nan Rosenbloom, Luke Van Roekel
Formal analysis: Gerald A. Meehl, Julie M. Arblaster, H. Annamalai

© 2023 The Authors.

This is an open access article under the terms of the [Creative Commons Attribution-NonCommercial License](#), which permits use, distribution and reproduction in any medium, provided the original work is properly cited and is not used for commercial purposes.

Gerald A. Meehl¹ , Christine A. Shields¹ , Julie M. Arblaster^{1,2} , Richard Neale¹ , Aixue Hu¹ , H. Annamalai³, Jean-Christophe Golaz⁴ , John Fasullo¹ , Nan Rosenbloom¹ , Luke Van Roekel⁵ , and Antonietta Capotondi⁶ 

¹National Center for Atmospheric Research, Boulder, CO, USA, ²ARC Centre of Excellence for Climate Extremes, Monash University, Melbourne, VIC, Australia, ³IPRC/Department of Oceanography, University of Hawaii at Manoa, Honolulu, HI, USA, ⁴Lawrence Livermore National Laboratory, Livermore, CA, USA, ⁵Los Alamos National Laboratory, Los Alamos, NM, USA, ⁶CIRES and NOAA Physical Sciences Laboratory, University of Colorado, Boulder, CO, USA

Abstract The effects of differences in climate base state are related to processes associated with the present-day South Asian monsoon simulations in the Energy Exascale Earth System Model version 2 (E3SMv2) and the Community Earth System Model version 2 (CESM2). Though tropical Pacific and Indian Ocean base state sea surface temperatures (SSTs) are over 1°C cooler in E3SMv2 compared to CESM2, and there is an overall reduction of Indian sector precipitation, the pattern of South Asian monsoon precipitation is similar in the two models. Monsoon-ENSO teleconnections, dynamically linked by the large-scale east-west atmospheric circulation, are reduced in E3SMv2 compared to CESM2. In E3SMv2, this is related to cooler tropical SSTs and ENSO amplitude that is less than half that in CESM2. Comparison to a tropical Pacific pacemaker experiment shows, to a first order, that the base state SSTs and ENSO amplitude contribute roughly equally to lower amplitude monsoon-ENSO teleconnections in E3SMv2.

Plain Language Summary Two different Earth system models are analyzed to investigate how differences in simulated base state tropical sea surface temperatures (SSTs) and El Niño/Southern Oscillation (ENSO) amplitude affect the processes associated with the South Asian monsoon. Though tropical SSTs are over 1°C cooler in the Energy Exascale Earth System Model version 2 (E3SMv2) and there is overall reduced Indian sector precipitation, the regional pattern of South Asian monsoon precipitation is similar in the two models. More significantly, monsoon-ENSO teleconnections are reduced in E3SMv2 compared to Community Earth System Model version 2 (CESM2) due to cooler mean tropical SSTs combined with ENSO amplitude in E3SMv2 that is less than half that in CESM2.

1. Introduction

Given the socioeconomic importance of the South Asian monsoon to the lives of millions of people living across that region, it is critical to understand the processes that produce fluctuations in the amplitude and patterns of monsoon precipitation. It is only then that credible monsoon predictions are possible for the near-term on seasonal to decadal timescales, as well as longer term projections beyond decadal. When evaluating monsoon simulations by Earth system models, it has long been recognized that the simulation of the climate base states in individual models can affect the characteristics of the monsoon simulations in those respective models where details of those models' formulations are well known and are related to the monsoon simulations (Cook et al., 2012; Harrop et al., 2019; Meehl, Shields, et al., 2020; Meehl et al., 2006, 2012; Shields et al., 2016). The effects of climate base states have been studied across collections of models for possible changes to monsoon characteristics in a warmer climate (Annamalai et al., 2007; Li & Ting, 2015; Narsey et al., 2020) including connections to ENSO (McGregor et al., 2022). Changes in Indo-Pacific SSTs can produce precipitation anomalies that affect monsoon-ENSO connections through the large-scale east-west atmospheric circulation (Annamalai et al., 2013; Power et al., 2013). There is a model dependence on these connections (Annamalai et al., 2007; Li & Ting, 2015), though there is evidence that a warmer base state produces a strengthening of monsoon-ENSO connections (McGregor et al., 2022).

While previous studies have analyzed large multi-model ensembles, here we focus on two models, E3SMv2 and CESM2, to illustrate in more detail how differences in the simulation of the present-day climate base states can affect processes involved with the South Asian monsoon simulations and monsoon-ENSO connections in those

Investigation: Gerald A. Meehl, Christine A. Shields, Julie M. Arblaster, Richard Neale, Aixue Hu, H. Annamalai, Jean-Christophe Golaz, Nan Rosenbloom, Luke Van Roekel, Antonietta Capotondi

Methodology: Gerald A. Meehl, Christine A. Shields, Julie M. Arblaster, Richard Neale, John Fasullo

Project Administration: Nan Rosenbloom

Software: Christine A. Shields, Julie M. Arblaster, Aixue Hu, Jean-Christophe Golaz, John Fasullo, Nan Rosenbloom, Luke Van Roekel

Validation: Christine A. Shields, Antonietta Capotondi

Visualization: Christine A. Shields, Julie M. Arblaster, Richard Neale, Aixue Hu, John Fasullo

Writing – original draft: Gerald A. Meehl

Writing – review & editing: Gerald A. Meehl, Christine A. Shields, Julie M. Arblaster, Richard Neale, Aixue Hu, H. Annamalai, Jean-Christophe Golaz, John Fasullo, Nan Rosenbloom, Antonietta Capotondi

two models. So-called “two model analyses” have a long history in the literature (e.g., Baumhefner, 1976). A single model analysis is just that, model results produced with knowledge of only one model's representation of the climate system, but no larger interpretability context. A multi-model ensemble analysis (e.g., CMIP) is able to document phenomena from a large number of models, but with little information with regards to the physical processes in the different models. A two model analysis advances understanding in the context of a familiarity with the processes in the two models. This provides more well-informed insights into the relevant physical mechanisms that emerge from analyses of those processes in the two models.

We pose a hypothesis based on the analyses of Bonfils et al. (2015), Katzenberger et al. (2021), and McGregor et al. (2022) that monsoon-ENSO connections would be stronger both due to the warmer base state SSTs and the larger amplitude ENSO in CESM2 compared to E3SMv2.

2. Models

The horizontal resolution configuration of E3SMv2 analyzed here consists of a 110-km atmosphere, 165-km land, 0.5° river model, and an ocean and sea ice with mesh spacing varying between 60 km in the mid-latitudes and 30 km at the equator and poles (Golaz et al., 2022). The ocean represents the biggest physical difference between E3SMv2 and CESM2 in that E3SMv2 uses an MPAS-Ocean (Petersen et al., 2019) while CESM2 includes a conventional grid point ocean model, POP2, as discussed below.

The atmospheric model in CESM2, as in E3SMv2, has a nominal 1° latitude-longitude resolution (Danabasoglu et al., 2020). The ocean model in CESM2 is a version of POP2 (Parallel Ocean Program, version 2) used in CESM1 but with many improvements to the physics (Danabasoglu et al., 2020). The POP2 ocean has a nominal one degree horizontal resolution and enhanced resolution in the equatorial tropics, and 60 levels in the vertical with ocean biogeochemistry. While the meridional resolution in the MPAS ocean in E3SMv2 is very similar to POP2 in CESM2, the grid cells are much more isotropic. This gives the MPAS ocean in E3SMv2 a much higher effective resolution than that in CESM2. A more full description of the two models is given in Supporting Information S1.

Pacemaker experiments with CESM2 (ten ensemble members) use time-evolving SST anomalies in the tropical Pacific nudged to observations (ERSSTv5, 1880–2019) whereby the observed evolution of ENSO is maintained along with the model's base state climate, while the rest of the model's coupled climate system is free to evolve (methodology described by Kosaka & Xie, 2013; Deser et al., 2017; Meehl, Hu, et al., 2020). More details of the pacemaker experiments are given in Supporting Information S1.

Experiments analyzed here are the historical simulations described in Danabasoglu et al. (2020) and Golaz et al. (2022) from 1850 to 2014. Both models have 20 ensemble members each. Analyses are performed for the South Asian monsoon season June-July-August-September (JJAS). Teleconnections between ENSO and the South Asian monsoon are calculated as running 13-year correlations between JJAS All-India Rainfall (defined as area-averaged rainfall over land grid points, 5°N–40°N, 60°E–100°E) and Niño3.4 SSTs (area-averaged SSTs in the eastern equatorial Pacific, 5°N–5°S, 170°W–120°W). To make the dynamical connection between the monsoon and ENSO, Niño3.4 time series are regressed onto 200 hPa velocity potential for the JJAS season. Additional analyses of the CMIP6 models also include Niño4 SSTs (5°N–5°S, 160°E–150°W).

3. Results

Figure 1 contrasts the seasonal mean climate base states in June-July-August-September (JJAS) in the two models as differences for E3SMv2 minus CESM2. E3SMv2 simulates tropical SSTs around 0.5°C cooler than observations (Golaz et al., 2022) while CESM2 has tropical SSTs at least 0.5°C warmer-than-observed (Danabasoglu et al., 2020). Therefore, differences for E3SMv2 minus CESM2 show negative tropical SST anomalies of over 1°C (Figure 1a). There is little change in SST gradients across the equatorial Indian and Pacific Oceans since there are nearly uniform SST anomalies there of about –1°C across the two ocean basins. As a consequence, E3SMv2 has generally reduced JJAS precipitation in the tropical Indian and Pacific sectors compared to CESM2 (Figure 1b) as previously noted (Danabasoglu et al., 2020; Golaz et al., 2022). There are negative precipitation anomalies for E3SMv2 minus CESM2 of about –1.5 mm day⁻¹ (roughly 15%–20%) in the tropical Indian Ocean, southern India, Myanmar, Indonesia, southeastern China, and the central equatorial Pacific (Figure 1b).

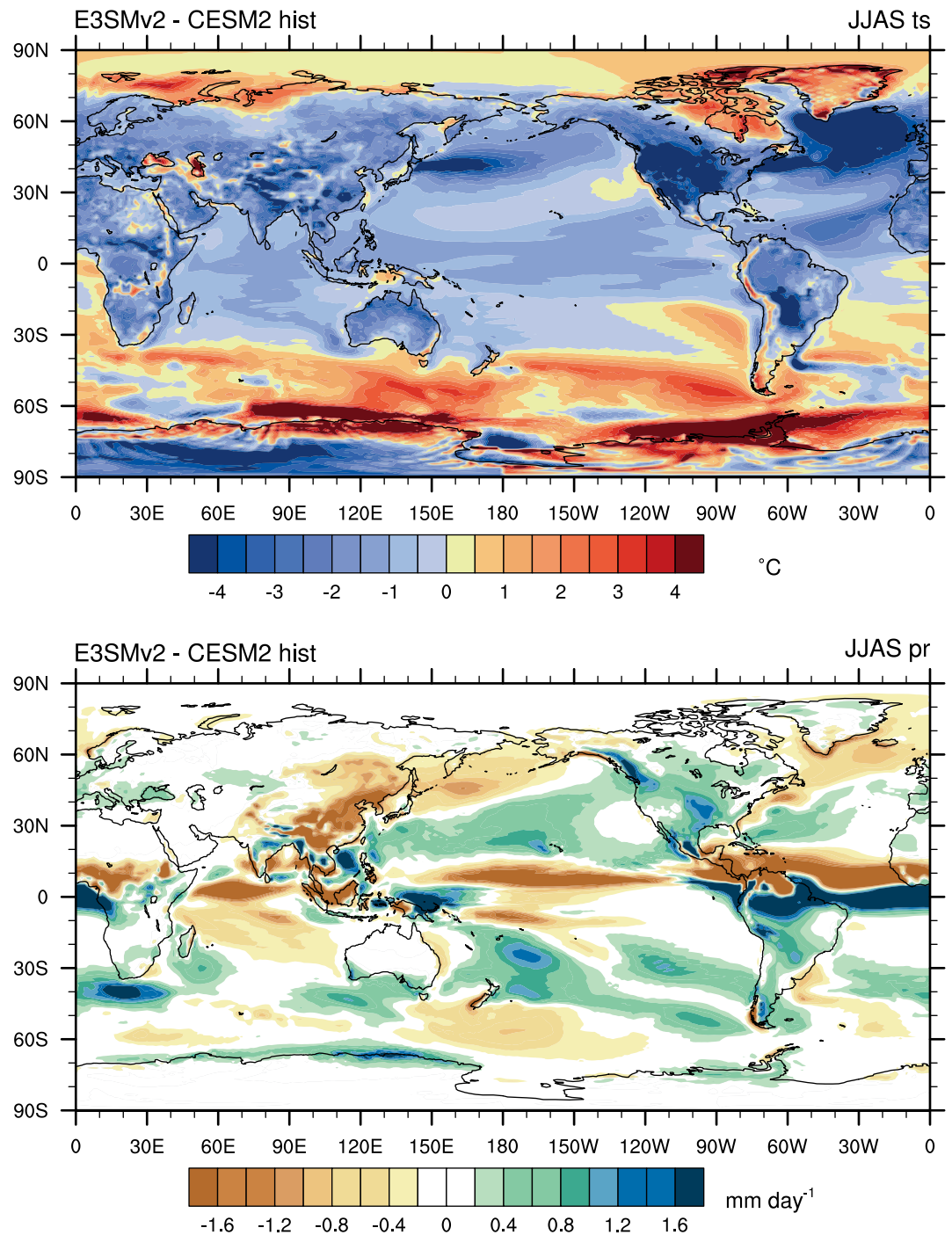


Figure 1. Mean base state differences for E3SMv2 minus CESM2, JJAS, 1995–2014, for (a) surface temperature ($^{\circ}\text{C}$), differences greater than about $\pm 0.5^{\circ}\text{C}$ are significant at the 99% level; and (b) precipitation (mm day^{-1}), differences greater than about $\pm 0.2 \text{ mm day}^{-1}$ are significant at the 99% level.

However, these differences in base state SSTs and precipitation do not translate into large differences in the *patterns* of simulated monsoon rainfall. Figures 2a–2c show monsoon precipitation and 850 hPa wind for seasonal mean (JJAS) simulations for E3SMv2, CESM2, and observations. Most previous versions of Earth system models simulate precipitation maxima that extend too far west in the western Indian Ocean (e.g., Meehl, Shields, et al., 2020; Meehl et al., 2012). E3SMv2 and CESM2 also have this error when compared to observations (Figures 2e and 2f) with positive differences in the western Indian Ocean. Additionally, basin maxima of

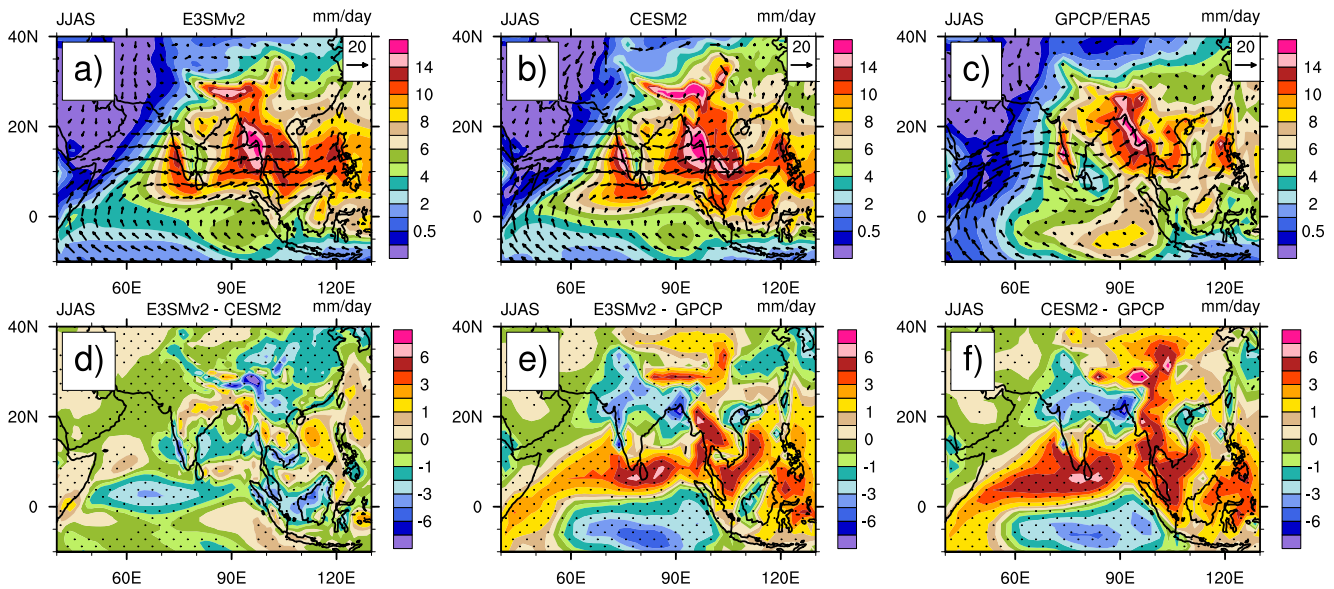


Figure 2. South Asian monsoon precipitation (mm day^{-1}) and 850-hPa wind vectors (m s^{-1}) for JJAS, 1995–2014; scaling arrow at upper right (a) E3SMv2, (b) CESM2, and (c) observations (GPCP/ERA-5); (d) precipitation differences, E3SMv2 minus CESM2; panel (e) same as (d) except for E3SMv2 minus observations; (f) same as (e) except for CESM2 minus observations; Stippling in (d)–(f) represents statistically significant differences at the 99% level using a student T -test. Wind data from the model was interpolated to 850 hPa and therefore is masked out over the Himalayas.

precipitation are too far upstream to the west of the main orographic features in the Arabian Sea and the Bay of Bengal. Also, as in previous model versions, the observed precipitation maximum near 5°S in Figure 2c is not well simulated in either model, with negative differences near 5°S in both (Figures 2e and 2f).

Precipitation maxima over the monsoon region in both models compared to observations have negative anomalies over northern India, but positive anomalies over southern India, Sri Lanka, the Himalayas, Myanmar and Thailand (Figures 2e and 2f). In general, these larger-than-observed precipitation anomalies are manifested by greater-than-observed vertically integrated moisture transports (IVT) in both models compared to observations (Figure S1 in Supporting Information S1). IVT values in CESM2 are greater than E3SMv2, and both are greater than observations, with a greater extent of values of nearly $600 \text{ kg m}^{-1} \text{ s}^{-1}$ compared to observed values of about $450 \text{ kg m}^{-1} \text{ s}^{-1}$ extending from the Arabian Sea across southern India to the Bay of Bengal. Neither model is able to capture the northward penetration of IVT into northern India seen in the observations. This southward-shifted concentration of IVT is a reflection of the greater-than-observed precipitation over southern India in both models (Figures 2e and 2f).

Even with these differences in the magnitude of the precipitation anomalies, the similarity of the precipitation patterns in both models is indicated by spatial pattern correlations between the two over the South Asian monsoon region depicted in Figure 2 of +0.95. The pattern correlations with observations over the South Asian monsoon region are +0.89 and +0.91 for E3SMv2 and CESM2, respectively. While there is a somewhat lower RMSE in E3SMv2 (2.19) compared to CESM2 (2.48) over the monsoon region, the differences in base state SST and precipitation shown in Figure 1 do not materially affect the patterns of precipitation over the South Asian monsoon region.

The northward progression of monthly mean precipitation over the South Asian monsoon region from 70°E – 100°E reflects the precipitation errors in both models. There is a similar seasonal progression of monthly mean precipitation, though the July precipitation maxima near 15°N is less in E3SMv2 (about 12 mm day^{-1}) compared to CESM2 (roughly 14 mm day^{-1}), and both of these maxima are less than observed (about 11 mm day^{-1}) and south of the observed maximum near 20 – 25°N (Figure S2 in Supporting Information S1). This is associated with the somewhat reduced amplitude of monsoon precipitation in E3SMv2 compared to CESM2 and the cooler tropical Indian Ocean SSTs in the E3SMv2.

To address monsoon-ENSO connections, Figure 3a shows running 13 years correlations between the observed JJAS All-India Rainfall (AIR, averaged over India) and the observed JJAS Niño3.4 SSTs, and comparable plots

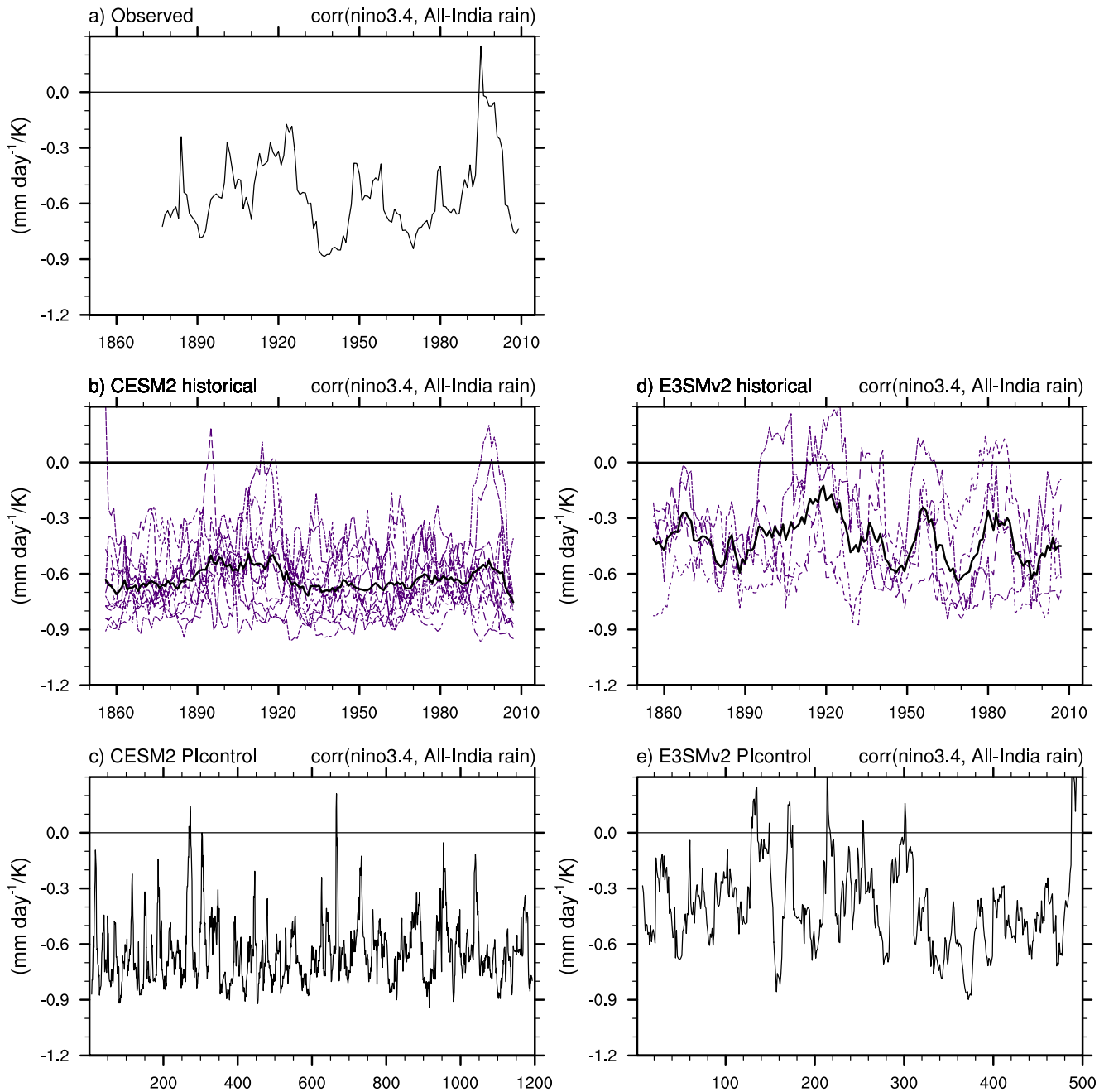


Figure 3. Running 13-year correlations between JJAS All-India Rainfall (AIR) and Niño3.4 SSTs for (a) observations (HadISST), (b) individual ensemble members from the CESM2 historical simulation, with the ensemble mean in black; and (c) years 1–1200 from the CESM2 pre-industrial control run; (d) same as (b) except for E3SMv2; panel (e) same as (c) except for 500 years from the E3SMv2 pre-industrial control run.

for historical simulations from the models in Figures 3b and 3d where AIR is defined as rainfall averaged over land points 5°N–40°N, 60°E–100°E. Both models show negative correlation values, as do the observations, indicating the well-known relationship between El Niño events and reduced monsoon precipitation (e.g., Rasmusson & Carpenter, 1983) and vice versa for La Niña events. E3SMv2 shows weaker correlations averaging -0.42 (Figure 3d) compared to -0.63 for CESM2 (Figure 3b), and -0.55 for observations (Figure 3a). The difference in correlations between the models is statistically significant with $p < 0.01$. Observed correlations range from about -0.9 to $+0.2$ (Figure 3a), while CESM2 has a similar range. The E3SMv2, with its smaller average correlations, also has an upward-shifted range of values from about -0.8 to $+0.3$ (Figure 3d). Therefore, these results indicate that the E3SMv2 has a weaker monsoon-ENSO connection compared to CESM2.

Nino34 regressions with 200 hPa CHI (velocity potential) JJAS
Nino 3.4 onto 200mb chi units . $\times 10^6 \text{ m}^2/\text{s} / \text{degC}$

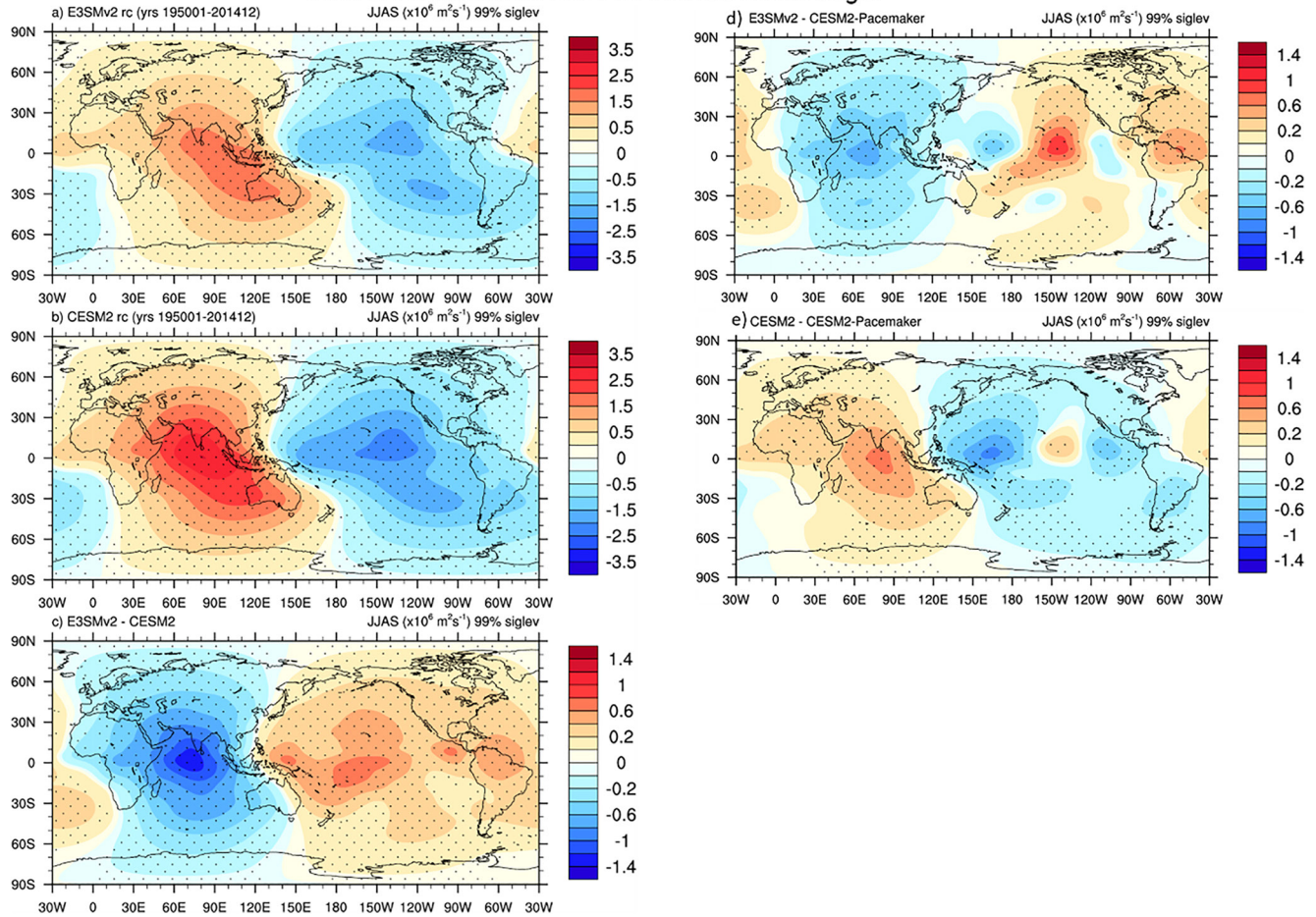


Figure 4. Niño3.4 time series regressed onto 200 hPa velocity potential, 1950–2014, season average JJAS ($\times 10^6 \text{ m}^2 \text{ sec}^{-2}/^\circ\text{C}$), (a) E3SMv2, (b) CESM2, (c) differences, E3SMv2 minus CESM2, (d) E3SMv2 values from panel (a) minus CESM2 pacemaker, and (e) CESM2 values from panel (b) minus CESM2 pacemaker. Stippling indicates 99% significance using a student *T*-test.

To put the models' monsoon-ENSO connections into a longer-term context, Figures 3c and 3e show values from the long pre-industrial control runs for CESM2 and E3SMv2, respectively. By construction, only internal variability can affect the results since there are no changes in external forcings in these simulations. Both are close to the magnitudes of the correlations in the respective historical runs in Figures 3b and 3d, with CESM2 having a larger amplitude average correlation of -0.64 compared to E3SMv2 with a smaller amplitude correlation of -0.40 . The difference between the correlation values from the two models is statistically significant with $p < 0.01$. Thus, there are weaker (in general) monsoon-ENSO correlations in E3SMv2 compared to CESM2 in both the historical and pre-industrial control runs, suggesting that monsoon-ENSO processes are being affected by either differences in model formulations or model base state climate simulations.

The processes that connect the monsoon and ENSO involve well-known dynamics of the large-scale east-west atmospheric circulation (the Walker Circulation) between the Pacific and Indian sectors (e.g., Meehl, 1987; Rasmusson & Carpenter, 1983). To illustrate these processes, Figures 4a and 4b show the regression of Niño3.4 SST on 200 hPa velocity potential for the two models. Both models show similar patterns that are seen in observations (e.g., Gill et al., 2015). There are negative values over the Pacific sector indicating, for El Niño events, anomalous upper level divergence associated with warmer SSTs and stronger precipitation and upward vertical motion there. Over the Indian sector, there are positive values denoting anomalous upper level convergence producing stronger downward vertical motion that acts to suppress monsoon precipitation. It is this connection via the large-scale east-west atmospheric circulation that produces the negative correlations between monsoon rainfall and Niño3.4 SSTs seen in Figure 3.

As has been previously documented, both models have ENSO SST centers of action in the equatorial Pacific shifted somewhat westward as in most models (Capotondi et al., 2020; Golaz et al., 2022), so the locations of the negative centers of the 200 hPa velocity potential regressions in the tropical Pacific are roughly comparable between the two models (Figure 4). However, the amplitude of the regression maxima in CESM2 is about 50% larger than in E3SMv2. In the Pacific and Indian sectors, there are statistically significant anomalies in CESM2 in Figure 4b of about $-2.5 \times 10^6 \text{ m}^2 \text{ sec}^{-2}/^\circ\text{C}$, and $+2.5 \times 10^6 \text{ m}^2 \text{ sec}^{-2}/^\circ\text{C}$, respectively, while in E3SMv2 in Figure 4a, those maxima are also statistically significant with values of roughly $-1.5 \times 10^6 \text{ m}^2 \text{ sec}^{-2}/^\circ\text{C}$ and $+1.5 \times 10^6 \text{ m}^2 \text{ sec}^{-2}/^\circ\text{C}$, respectively. This produces statistically significant differences for E3SMv2 minus CESM2 (Figure 4c) approaching $+1.0 \times 10^6 \text{ m}^2 \text{ sec}^{-2}/^\circ\text{C}$ over the tropical Pacific and over $-1.0 \times 10^6 \text{ m}^2 \text{ sec}^{-2}/^\circ\text{C}$ in the Indian sector. The negative differences over the Indian sector and positive differences over the Pacific in Figure 4c are indicative of the weaker monsoon-ENSO connection in E3SMv2 compared to CESM2 consistent with results in Figure 3.

The reason for this stronger connection in CESM2 compared to E3SMv2 is likely twofold. First, the warmer base state SSTs in CESM2 provide a stronger large-scale east-west connection through the well-documented non-linear relationship between SST and precipitation that would produce stronger convective maxima during ENSO events and thus a stronger forcing through the large-scale east-west circulation (e.g., Bonfils et al., 2015; McGregor et al., 2022; Power et al., 2013; Yun et al., 2021). Second, CESM2 has over twice the amplitude of ENSO than E3SMv2 (Figure S3 in Supporting Information S1), and other studies have shown evidence for larger amplitude ENSO with a warmer base state climate (Cai et al., 2021, 2022). Therefore, the results from CESM2 and E3SMv2 are consistent with previous findings that larger amplitude ENSO, combined with warmer base state SSTs, can force stronger large-scale east-west connections between Pacific and Indian sectors (e.g., Bonfils et al., 2015; Turner et al., 2005).

To isolate the influence of each of these processes, model experiments using the tropical Pacific pacemaker methodology in CESM2 described earlier (and in Supporting Information S1) are analyzed. Of relevance to this analysis, only the SST anomalies over the tropical Pacific, not the total SSTs, are nudged to observations, thus maintaining the model's climate basic state. Therefore, ENSO amplitude is as observed by construction, is reduced in the pacemaker experiment compared to the standard CESM2 version, and is close to that in E3SMv2 (Figure S3 in Supporting Information S1). Meanwhile, the mean tropical SSTs in the pacemaker experiment remain over 1°C warmer than E3SMv2. In this way, with the caveat that these are somewhat different models and configurations, the relative influences of cooler tropical SSTs or reduced ENSO amplitude can be isolated, to a first order, with regards to monsoon-ENSO connections.

The differences between the E3SMv2 and the CESM2 pacemaker in Figure 4d show statistically significant negative anomalies over the Indian sector of about $-0.6 \times 10^6 \text{ m}^2 \text{ sec}^{-2}/^\circ\text{C}$, and mostly positive anomalies, when taken over the entire Pacific sector, averaging around $+0.4 \times 10^6 \text{ m}^2 \text{ sec}^{-2}/^\circ\text{C}$. This result indicates that the effect of colder tropical Pacific SSTs in E3SMv2, but with the same ENSO amplitude as in the Pacific pacemaker experiment, produce a weaker monsoon-ENSO connection. Conversely the differences between the CESM2 and the pacemaker experiment in Figure 4e show significant positive anomalies of around $+0.6 \times 10^6 \text{ m}^2 \text{ sec}^{-2}/^\circ\text{C}$ over the Indian sector, and mostly negative anomalies, when taken over the entire Pacific sector, averaging around $-0.4 \times 10^6 \text{ m}^2 \text{ sec}^{-2}/^\circ\text{C}$. Therefore, the effect of greater ENSO amplitude in the standard CESM2 compared to the specified observed ENSO amplitude in the pacemaker experiment, but with the same base state tropical SSTs, is a stronger monsoon-ENSO connection. Since the total of the simulations with both effects together in Figure 4c is statistically significant with values of about $-1.2 \times 10^6 \text{ m}^2 \text{ sec}^{-2}/^\circ\text{C}$ over the Indian sector and around $+0.8 \times 10^6 \text{ m}^2 \text{ sec}^{-2}/^\circ\text{C}$ over the Pacific sector, the differences using the pacemaker experiment as the reference in Figures 4d and 4e show significant respective differences about half that for the total in Figure 4c. These results suggest that, for these models to a first order, the reduced monsoon-ENSO connection in E3SMv2 compared to CESM2 is about half due to the colder base state tropical SSTs in E3SM, and half due to the reduced ENSO amplitude in E3SMv2.

4. Broader Implications

The connections documented above for E3SMv2 and CESM2, whereby there is a stronger monsoon-ENSO connection in the model with larger amplitude ENSO and warmer average Pacific SSTs, can be demonstrated for a larger group of 56 CMIP6 models (Figure S4 in Supporting Information S1). Figure S4a in Supporting

Information S1 shows the correlation between the inter-model spreads of annual mean SST at each grid point and the strength of their respective South Asian monsoon rainfall–Niño4 correlations averaged over 1950–2014. Over most of the tropical Pacific and Indian Oceans, the correlations are negative, indicating that stronger negative correlations between South Asian monsoon rainfall and tropical Pacific SST are associated with warmer annual mean SST. Statistically significant values are shifted to the west in the tropical Pacific, indicative of the well-known systematic error noted above that is present in the CMIP6 models of an over-extensive Pacific cold tongue, and thus stronger connections of the monsoon–ENSO connection farther to the west. This systematic model error is reflected in the scatter plots in Figures S4b and S4c in Supporting Information S1 for standard deviation of Niño3.4 and Niño4 SSTs plotted as a function of the respective monsoon–ENSO correlations. There is a stronger relationship for Niño4 that is farther west (Figure S4c in Supporting Information S1) than for Niño3.4 (Figure S4b in Supporting Information S1). Both have statistically significant r values, but Niño4 in Figure S4c in Supporting Information S1 is larger with $r = -0.46$. Therefore, the relationships shown for the two models in the present paper can be generalized, to first order, to this larger group of climate models, whereby larger Pacific ENSO SST variability and warmer average tropical Pacific SSTs are associated with stronger monsoon–ENSO connections.

Acknowledgments

Portions of this study were supported by the Regional and Global Model Analysis (RGMA) component of the Earth and Environmental System Modeling Program of the U.S. Department of Energy's Office of Biological and Environmental Research (BER) under Award Number DE-SC0022070. This work also was supported by the National Center for Atmospheric Research, which is a major facility sponsored by the National Science Foundation (NSF) under Cooperative Agreement No. 1852977. The Energy Exascale Earth System Model (E3SM) project is funded by the U.S. Department of Energy, Office of Science, Office of Biological and Environmental Research (BER). E3SM production simulations were performed on a high-performance computing cluster provided by the BER Earth System Modeling program and operated by the Laboratory Computing Resource Center at Argonne National Laboratory. Developmental simulations, as well as post-processing and data archiving of production simulations used resources of the National Energy Research Scientific Computing Center (NERSC), a DOE Office of Science User Facility supported by the Office of Science of the U.S. Department of Energy under Contract No. DE-AC02-05CH11231. The CESM project is supported primarily by the National Science Foundation (NSF). Computing and data storage resources, including the Cheyenne supercomputer, were used for the CESM simulations (<https://doi.org/10.5065/D6RX99HX>). H. Annamalai is supported by an NSF project under Grant 1460742. A. Capotondi was supported by DOE Award #DE-SC0023228. Lawrence Livermore National Laboratory is operated by Lawrence Livermore National Security, LLC, for the U.S. Department of Energy, National Nuclear Security Administration under Contract DE-AC52-07NA27344. We acknowledge the World Climate Research Programme, which, through its Working Group on Coupled Modelling, coordinated and promoted CMIP6. We thank the climate modeling groups for producing and making available their model output, the Earth System Grid Federation (ESGF) for archiving the data and providing access, and the multiple funding agencies who support CMIP6 and ESGF.

Data Availability Statement

E3SMv2 model code and tools may be accessed on the GitHub repository at <https://github.com/E3SM-Project/E3SM>. A maintenance branch (maint-2.0; <https://github.com/E3SM-Project/E3SM/tree/maint-2.0>) has been specifically created to reproduce E3SMv2 simulations. Complete native model output is accessible directly on NERSC at <https://portal.nersc.gov/archive/home/projects/e3sm/www/WaterCycle/E3SMv2/LR>. A subset of the data reformatted following CMIP conventions is available through the DOE Earth System Grid Federation (ESGF) at <https://esgf-node.llnl.gov/projects/e3sm>. The CESM2 solutions/data sets used in this study are available from the Earth System Grid Federation (ESGF) at esgf-node.llnl.gov/search/cmip6 or from the NCAR Digital Asset Services Hub (DASH) at data.ucar.edu or from the links provided from the CESM web site at www.cesm.ucar.edu. The pacemaker experiments with CESM2 are available at <https://www.cesm.ucar.edu/working-groups/climate/simulations/cesm2-pacific-pacemaker>. The All-India Rainfall is available from: https://data.gov.in/catalog/all-india-area-weighted-monthly-seasonal-and-annual-rainfall-mm?filters%5Bfield_catalog_reference%5D=85825&format=json&offset=0&limit=6&sort%5Bcreated%5D=desc. The ERA-5 data (Hersbach et al., 2020) are available from: <https://www.ecmwf.int/en/forecasts/dataset/ecmwf-reanalysis-v5>. ERSSTv5 data are available from: <https://psl.noaa.gov/data/gridded/data.noaa.ersst.v5.html/>. HADiSST data are available from: <https://www.metoffice.gov.uk/hadobs/hadisst/>. MERRA2 data from 1980 to 2015 (<https://doi.org/10.5065/D62R3QFS>). GPCP rainfall data (Adler et al., 2003) are from <https://www.esrl.noaa.gov/psd/data/gridded/data.gpcp.html>.

References

- Adler, R. F., Huffman, G. J., Chang, A., Ferraro, R., Xie, P. P., Janowiak, J., et al. (2003). The Version 2 global precipitation climatology project (GPCP) monthly precipitation analysis (1979–Present). *Journal of Hydrometeorology*, 4(6), 1147–1167. [https://doi.org/10.1175/1525-7541\(2003\)004<1147:tvGPCP>2.0.CO;2](https://doi.org/10.1175/1525-7541(2003)004<1147:tvGPCP>2.0.CO;2)
- Annamalai, H., Hafner, J., Sooraj, K. P., & Pillai, P. (2013). Global warming shifts the monsoon circulation, drying South Asia. *Journal of Climate*, 26(9), 2701–2718. <https://doi.org/10.1175/JCLI-D-12-00208.1>
- Annamalai, H., Hamilton, K., & Sperber, K. R. (2007). South Asian summer monsoon and its relationship with ENSO in the IPCC AR4 simulations. *Journal of Climate*, 20(6), 1071–1092. <https://doi.org/10.1175/jcli4035.1>
- Baumhufner, D. (1976). A single forecast comparison between the NCAR and GFDL general circulation models. *Monthly Weather Review*, 104(9), 1175–1177. [https://doi.org/10.1175/1520-0493\(1976\)104<1175:ASFBCBT>2.0.CO;2](https://doi.org/10.1175/1520-0493(1976)104<1175:ASFBCBT>2.0.CO;2)
- Bonfils, C. J. W., Santer, B. D., Phillips, T. J., Marvel, K., Leung, L. R., Doutriaux, C., & Capotondi, A. (2015). Relative contributions of mean-state shifts and ENSO-driven variability to precipitation changes in a warming climate. *Journal of Climate*, 28(24), 9997–10013. <https://doi.org/10.1175/JCLI-D-15-0341.1>
- Cai, W., Ng, B., Wang, G., Santoso, A., Wu, L., & Yang, K. (2022). Increased ENSO sea surface temperature variability under four IPCC emission scenarios. *Nature Climate Change*, 12(3), 228–231. <https://doi.org/10.1038/S31558-022-01282-z>
- Cai, W., Santoso, A., Collins, M., Dewitte, B., Karamperidou, C., Kug, J. S., et al. (2021). Changing El Niño–Southern Oscillation in a warming climate. *Nature Reviews Earth & Environment*, 2(9), 628–644. <https://doi.org/10.1038/S33017-021-00199-z>
- Capotondi, A., Deser, C., Phillips, A. S., Okumura, Y., & Larson, S. M. (2020). ENSO and Pacific decadal variability in CESM2. *Journal of Advances in Modeling Earth Systems*, 12(12), e2019MS002022. <https://doi.org/10.1029/2019MS002022>
- Cook, K. H., Meehl, G. A., & Arblaster, J. M. (2012). Monsoon regimes and processes in CCSM4. Part 2: The African and American monsoons. *Journal of Climate*, 25(8), 2609–2621. <https://doi.org/10.1175/JCLI-D-11-00185.1>
- Danabasoglu, G., Lamarque, J., Bacmeister, J., Bailey, D. A., DuVivier, A. K., Edwards, J., et al. (2020). The community Earth system model version 2 (CESM2). *Journal of Advances in Modeling Earth Systems*, 12, e2019MS001916. <https://doi.org/10.1029/2019MS001916>

- Deser, C., Guo, R., & Lehner, F. (2017). The relative contributions of tropical Pacific sea surface temperatures and atmospheric internal variability to the recent global warming hiatus. *Geophysical Research Letters*, *44*(15), 7945–7954. <https://doi.org/10.1002/2017GL074273>
- Gill, E. C., Rajagopalan, B., & Molnar, P. (2015). Subseasonal variations in spatial signatures of ENSO on the Indian summer monsoon from 1901 to 2009. *Journal of Geophysical Research: Atmospheres*, *120*(16), 8165–8185. <https://doi.org/10.1002/2015JD023184>
- Golaz, J.-C., Van Roekel, L. P., Zheng, X., Roberts, A. F., Wolfe, J. D., Lin, W., et al. (2022). The DOE E3SM model version 2: Overview of the physical model. *Journal of Advances in Modeling Earth Systems*, *14*(12), e2022MS003156. <https://doi.org/10.1029/2022MS003156>
- Harrop, B. E., Ma, P.-L., Rasch, P. J., Qian, Y., Lin, G., & Hannay, C. (2019). Understanding monsoonal water cycle changes in a warmer climate in E3SMv1 using a normalized gross moist stability framework. *Journal of Geophysical Research: Atmospheres*, *124*(20), 10826–10843. <https://doi.org/10.1029/2019JD031443>
- Hersbach, H., Bell, B., Berrisford, P., Hirahara, S., Horányi, A., Muñoz-Sabater, J., et al. (2020). The ERA5 global reanalysis. *Quarterly Journal of the Royal Meteorological Society*, *146*(730), 1999–2049. <https://doi.org/10.1002/qj.3803>
- Katzenberger, A., Schewe, J., Pongratz, J., & Levermann, A. (2021). Robust increase of Indian monsoon rainfall and its variability under future warming in CMIP6 models. *Earth System Dynamics*, *12*(2), 367–386. <https://doi.org/10.5194/esd-12-367-2021>
- Kosaka, Y., & Xie, S.-P. (2013). Recent global-warming hiatus tied to equatorial Pacific surface cooling. *Nature*, *501*(7467), 403–407. <https://doi.org/10.1038/nature12534>
- Li, X., & Ting, M. (2015). Recent and future changes in the Asian monsoon-ENSO relationship: Natural or forced? *Geophysical Research Letters*, *42*(9), 3502–3512. <https://doi.org/10.1002/2015GL063557>
- McGregor, S., Cassou, C., Kosaka, Y., & Phillips, A. S. (2022). Projected ENSO teleconnection changes in CMIP6. *Geophysical Research Letters*, *49*(11), e2021GL097511. <https://doi.org/10.1029/2021GL097511>
- Meehl, G. A. (1987). The annual cycle and interannual variability in the tropical Pacific and Indian Ocean regions. *Monthly Weather Review*, *115*(1), 27–50. [https://doi.org/10.1175/1520-0493\(1987\)115<0027:tacaiv>2.0.co;2](https://doi.org/10.1175/1520-0493(1987)115<0027:tacaiv>2.0.co;2)
- Meehl, G. A., Arblaster, J. M., Caron, J., Annamalai, H., Jochum, M., Chakraborty, A., & Murtugudde, R. (2012). Monsoon regimes and processes in CCSM4. Part 1: The Asian-Australian monsoon. *Journal of Climate*, *25*(8), 2583–2608. <https://doi.org/10.1175/JCLI-D-11-00184.1>
- Meehl, G. A., Arblaster, J. M., Lawrence, D., Seth, A., Schneider, E. K., Kirtman, B. P., & Min, D. (2006). Monsoon regimes in the CCSM3. *Journal of Climate*, *19*(11), 2482–2495. <https://doi.org/10.1175/jcli3745.1>
- Meehl, G. A., Shields, C., Arblaster, J. M., Annamalai, H., & Neale, R. (2020). Intraseasonal, seasonal, and interannual characteristics of regional monsoon simulations in CESM2. *Journal of Advances in Modeling Earth Systems*, *12*(6), e2019MS001962. <https://doi.org/10.1029/2019MS001962>
- Meehl, G. A., Hu, A., Castruccio, F., England, M. H., Bates, S. C., Danabasoglu, G., et al. (2020). Atlantic and Pacific tropics connected by mutually interactive decadal-timescale processes. *Nature Geoscience*, *14*(1), 36–42. <https://doi.org/10.1038/S31561-020-00669-x>
- Narsey, S. Y., Brown, J. R., Colman, R. A., Delage, F., Power, S. B., Moise, A. F., & Zhang, H. (2020). Climate change projections for the Australian monsoon from CMIP6 models. *Geophysical Research Letters*, *47*(13), e2019GL086816. <https://doi.org/10.1029/2019GL086816>
- Petersen, M. R., Asay-Davis, X. S., Berres, A. S., Chen, Q., Feige, N., Hoffman, M. J., et al. (2019). An evaluation of the ocean and sea ice climate of E3SM using MPAS and interannual CORE-II forcing. *Journal of Advances in Modeling Earth Systems*, *11*(5), 1438–1458. <https://doi.org/10.1029/2018MS001373>
- Power, S., Delage, F., Chung, C., Kociuba, G., & Keay, K. (2013). Robust twenty-first-century projections of El Niño and related precipitation variability. *Nature*, *502*(7472), 541–545. <https://doi.org/10.1038/nature12580>
- Rasmusson, E. M., & Carpenter, T. H. (1983). The relationship between eastern equatorial Pacific sea surface temperature and rainfall over India and Sri Lanka. *Monthly Weather Review*, *111*(3), 517–528. [https://doi.org/10.1175/1520-0493\(1983\)111<0517:trbeep>2.0.co;2](https://doi.org/10.1175/1520-0493(1983)111<0517:trbeep>2.0.co;2)
- Shields, C. A., Kiehl, J. T., & Meehl, G. A. (2016). Future changes in regional precipitation simulated by a half-degree coupled climate model: Sensitivity to horizontal resolution. *Journal of Advances in Modeling Earth Systems*, *8*(2), 863–884. <https://doi.org/10.1002/2015MS000584>
- Turner, A. G., Inness, P. M., & Slingo, J. M. (2005). The role of the basic state in the ENSO-monsoon relationship and implications for predictability. *Quarterly Journal of the Royal Meteorological Society*, *131*(607), 781–804. <https://doi.org/10.1256/qj.04.70>
- Yun, K.-S., Lee, J. Y., Timmermann, A., Stein, K., Stuecker, M. F., Fyfe, J. C., & Chung, E. S. (2021). Increasing ENSO–rainfall variability due to changes in future tropical temperature–rainfall relationship. *Communications Earth & Environment*, *2*(1), 43. <https://doi.org/10.1038/S33247-021-00108-8>

References From the Supporting Information

- Beljaars, A. C. M., Brown, A. R., & Wood, N. (2004). A new parametrization of turbulent orographic form drag. *The Quarterly Journal of the Royal Meteorological Society*, *130*(599), 1327–1347. <https://doi.org/10.1256/qj.o3.73>
- Bradley, A. M., Bosler, P. A., & Guba, O. (2021). Islet: Interpolation semi-Lagrangian element-based transport. *Geoscientific Model Development Discussions*, 1–48. <https://doi.org/10.5194/gmd-2021-296>
- Gottelman, A., & Morrison, H. (2015). Advanced two-moment bulk microphysics for global models. Part I: Off-line tests and comparison with other schemes. *Journal of Climate*, *28*(3), 1268–1287. <https://doi.org/10.1175/JCLI-D-14-00102.1>
- Gnanadesikan, A., Russell, A., Pradal, M.-A., & Abernathy, R. (2017). Impact of lateral mixing in the ocean on El Niño in a suite of fully coupled climate models. *Journal of Advances in Modeling Earth Systems*, *9*(7), 2493–2513. <https://doi.org/10.1002/2017MS000917>
- Golaz, J.-C., Caldwell, P. M., Van Roekel, L. P., Petersen, M. R., Tang, Q., Wolfe, J. D., et al. (2019). The DOE E3SM coupled model version 1: Overview and evaluation at standard resolution. *Journal of Advances in Modeling Earth Systems*, *11*(7), 2089–2129. <https://doi.org/10.1029/2018ms001603>
- Harrop, B. E., Ma, P.-L., Rasch, P. J., Neale, R. B., & Hannay, C. (2018). The role of convective gustiness in reducing seasonal precipitation biases in the tropical West Pacific. *Journal of Advances in Modeling Earth Systems*, *1*(4), 1–10. <https://doi.org/10.1002/2017MS001157>
- Hurrell, J. W., Holland, M. M., Gent, P. R., Ghan, S., Kay, J. E., Kushner, P. J., et al. (2013). The community Earth system model: A framework for collaborative research. *Bulletin American Meteorology Society*, *94*(9), 1339–1360. <https://doi.org/10.1175/bams-d-12-00121.1>
- Knutti, R., Sedláček, J., Sanderson, B. M., Lorenz, R., Fischer, E., & Eyring, V. (2017). A climate model projection weighting scheme accounting for performance and interdependence. *Geophysical Research Letters*, *44*, 1909–1918. <https://doi.org/10.1002/2016GL072012>
- Larson, V. E. (2017). CLUBB-SILHS: A parameterization of subgrid variability in the atmosphere. arXiv, 1711.03675v4. <https://doi.org/10.48550/ARXIV.1711.03675>
- Liu, X., Ma, P.-L., Wang, H., Tilmes, S., Singh, B., Easter, R. C., et al. (2016). Description and evaluation of a new four-mode version of the modal aerosol module (MAM4) within version 5.3 of the community atmosphere model. *Geoscientific Model Development*, *9*(2), 505–522. <https://doi.org/10.5194/gmd-9-505-2016>

- Ma, P.-L., Harrop, B. E., Larson, V. E., Neale, R. B., Gettelman, A., Morrison, H., et al. (2022). Better calibration of cloud parameterizations and subgrid effects increases the fidelity of E3SM Atmosphere Model version 1. *Geoscientific Model Development*, *15*(7), 2881–2916. <https://doi.org/10.5194/gmd-15-2881-2022>
- Neale, R. B., Richter, J. H., & Jochum, M. (2008). The impact of convection on ENSO: From a delayed oscillator to a series of events. *Journal of Climate*, *21*(22), 5904–5924. <https://doi.org/10.1175/2008JCLI2244.1>
- Smith, C. J., Kramer, R. J., Myhre, G., Alterskjær, K., Collins, W., Sima, A., et al. (2020). Effective radiative forcing and adjustments in CMIP6 models. *Atmospheric Chemistry and Physics*, *20*(16), 9591–9618. <https://doi.org/10.5194/acp-20-9591-2020>
- Taylor, M. A., Guba, O., Steyer, A., Ullrich, P. A., Hall, D. M., & Eldrid, C. (2020). An energy consistent discretization of the nonhydrostatic equations in primitive variables. *Journal of Advances in Modeling Earth Systems*, *12*(1), e2019MS001783. <https://doi.org/10.1029/2019MS001783>
- Xie, S., Wang, Y., Lin, W., Ma, H., Tang, Q., Tang, S., et al. (2019). Improved diurnal cycle of precipitation in E3SM with a revised convective triggering function. *Journal of Advances in Modeling Earth Systems*, *11*(7), 2290–2310. <https://doi.org/10.1029/2019MS001702>
- Zhang, G., & Mcfarlane, N. A. (1995). Sensitivity of climate simulations to the parameterization of cumulus convection in the Canadian Climate Centre general circulation model. *Atmosphere-Ocean*, *33*(3), 407–446. <https://doi.org/10.1080/07055900.1995.9649539>